Molecular Structure of Trifluorophosphine Tetraborane(8), $B_4H_8PF_3$, As Determined in the Gas Phase by Electron Diffraction and *ab Initio* Computations

Paul T. Brain, David W. H. Rankin,* and Heather E. Robertson

Department of Chemistry, University of Edinburgh, West Mains Road, Edinburgh, EH9 3JJ, U.K.

Mark A. Fox, Robert Greatrex,* and Alireza Nikrahi

School of Chemistry, University of Leeds, Leeds, LS2 9JT, U.K.

Michael Bühl

Institut für Organische Chemische, Universität Zürich,
Winterthurerstrasse 190, CH-8057, Zürich, Switzerland

Received August 22, 1996[⊗]

The molecular structure of trifluorophosphine tetraborane(8), $B_4H_8PF_3$, has been studied in the gas phase by electron diffraction. The experimental data can be fitted using a model which represents the gas as consisting solely of the *endo* conformer with C_s symmetry, the PF_3 group staggered with respect to the B(1)−H(1) bond. Important experimental structural parameters (r_α°) are *r*[B(1)−B(2)] (hinge−wing) = 184.7(9) pm, *r*[B(1)−B(3)] (hinge−hinge) = 172.2(12) pm, *r*[B(2)−B(3)] = 179.9(10) pm, *r*[B(1)−P] = 179.8(9) pm, and *r*(P−F) (mean) = 152.8(1) pm; B(3)B(1)P = 131.6(11)°, and the dihedral ("butterfly") angle between the planes B(1)B-(2)B(3) and B(1)B(4)B(3) is 133.9(23)°. These values agree well with the *ab initio* (MP2/TZP level) optimized molecular geometry for the *endo* conformer; at the MP2/TZP//MP2/TZP + ZPE(HF/6-31G*) level, the *exo* conformer is predicted to represent *ca*. 2% of the compound vapor, consistent with the experimental ^{11}B NMR solution spectrum. The experimental and theoretical geometries are supported by comparison of the calculated (IGLO) ^{11}B NMR chemical shifts with the experimental NMR data.

Introduction

Lewis-base adducts of tetraborane(8), B_4H_8L, exhibit interesting isomeric behavior, the nature of which has been investigated in some detail by NMR spectroscopic and X-ray crystallographic methods. For example, the adducts $B_4H_8PF_2X$ (X = F, Cl, NMe_2, OMe, SMe, ^{t}Bu) exist in solution as temperature-dependent mixtures of geometrical isomers (*endo* or *exo* placement of the ligand with respect to the folded B_4 framework—see below);[1−4] rotamers are observed at low temperatures for the *endo* isomers. By contrast, $B_4H_8PF_2H$ exists solely as the *endo* form,[4] as does $B_4H_8PF_2NMe_2$ in the crystalline state.[5] The only gas-phase structure has been determined for the adduct B_4H_8CO, in which rotational isomerism is not possible; the sample was found by electron diffraction to consist of a mixture of the *endo* and *exo* isomers in a ratio of 62:38.[6] Subsequently the *ab initio* optimized geometries of the two isomers were found to be in very good agreement with the experimentally determined values.[7] A theoretical study of the adducts B_4H_8L (L = CO, NH_3, PF_3, PH_3) has also been reported by Mebel *et al*.[8]

Chart 1

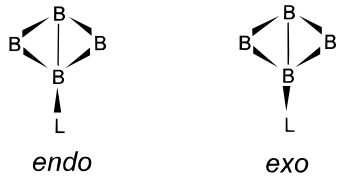

The factors that account for the stabilization of one isomer relative to another in compounds of this type are not fully understood, and it is by no means clear whether the *exo*:*endo* ratios are determined mainly by electronic considerations or by steric requirements of the ligands. To provide further insights, we have investigated the structure of $B_4H_8PF_3$ in the gas phase by electron diffraction (GED) and by *ab initio* computations, making use of the combined *ab initio*/IGLO/NMR method[9−12] to augment the structural determination. This approach has proved to be highly successful in studies of borane structures,[13] including those of the three B_4H_{10} derivatives 2,4-$(CH_2)_2B_4H_8$,[13c] 2,4-(MeCHCH$_2$)B_4H_8[13d] and 2,4-(*trans*-MeCHCHMe)B_4H_8.[13d]

* Authors to whom correspondence should be addressed.
[⊗] Abstract published in *Advance ACS Abstracts*, February 15, 1997.

(1) Paine, R. T.; Parry, R. W. *Inorg. Chem.* **1972**, *11*, 1237.
(2) Centofanti, L. F.; Kodama, G.; Parry, R. W. *Inorg. Chem.* **1969**, *8*, 2072.
(3) Odom, J. D.; Moore, T. F.; Dawson, W. H.; Garber, A. R.; Stampf, E. J. *Inorg. Chem.* **1979**, *18*, 2179.
(4) Odom, J. D.; Moore, T. F. *Inorg. Chem.* **1980**, *19*, 2651.
(5) La Prade, M. D.; Nordman, C. E. *Inorg. Chem.* **1969**, *8*, 1669.
(6) Cranson, S. J.; Davies, P. M.; Greatrex, R.; Rankin, D. W. H.; Robertson, H. E. *J. Chem. Soc., Dalton Trans.* **1990**, 101.
(7) Bühl, M.; Schleyer, P. v. R. *Struct. Chem.* **1993**, *4*, 1.
(8) Mebel, A. M.; Djamaladdin, G. M.; Morokuma, K. *Chem. Phys. Lett.* **1993**, *214*, 69.
(9) (a) Kutzelnigg, W. *Isr. J. Chem.* **1980**, *19*, 193. (b) Schindler, M.; Kutzelnigg, W. *J. Chem. Phys.* **1982**, *76*, 1919. (c) Review: Kutzelnigg, W.; Schindler, M.; Fleischer, U. In *NMR, Basic Principles and Progress*; Springer Verlag: Berlin, 1990; Vol. 23, p 165.
(10) Meier, U.; van Wüllen, C.; Schindler, M. *J. Comput. Chem.* **1992**, *13*, 551.
(11) Bühl, M.; Schleyer, P. v. R. *J. Am. Chem. Soc.* **1992**, *114*, 477.
(12) For examples of the application of the *ab initio*/IGLO/NMR method to boron compounds see: Diaz, M.; Jaballas, J.; Arias, J.; Lee, H.; Onak, T. *J. Am. Chem. Soc.* **1996**, *118*, 4405 and references therein.

S0020-1669(96)01032-4 CCC: $14.00

Table 1. Nozzle-to-Plate Distances, Weighting Functions, Correlation Parameters, Scale Factors, and Electron Wavelengths

nozzle-to-plate dist/mm	Δs/nm^{-1}	s_{min}/nm^{-1}	sw_1/nm^{-1}	sw_2/nm^{-1}	s_{max}/nm^{-1}	correln param	scale factor, k[a]	electron wavelength[b]/pm
285.8	2	20	40	122	144	0.438	0.595(9)	5.667
128.2	4	120	140	292	344	0.456	0.609(21)	5.667

[a] Figures in parentheses are the estimated standard deviations. [b] Determined by reference to the scattering pattern of benzene vapor.

Experimental Section

Synthesis. Trifluorophosphine tetraborane(8), $B_4H_8PF_3$, was prepared as suggested previously[14] by repeated reaction of B_4H_8CO and PF_3 (Aldrich) in a 75 cm^3 Hoke single-ended stainless-steel pressure tube. In each reaction, the tube was charged with B_4H_8CO (6 mmol) and PF_3 (12 bar) and held at 30 °C for 2 h. The volatile products were separated by low-temperature fractional distillation *in vacuo*, and the purity of the adduct was assessed by reference to its ^{1}H, ^{11}B, and ^{19}F NMR spectra;[4,15,16] a small amount of residual B_4H_8CO was shown to be present.[6]

Electron-Diffraction Measurements. Electron-scattering intensities were recorded on Kodak Electron Image plates using the Edinburgh gas-diffraction apparatus operating at *ca*. 44.5 kV (electron wavelength *ca*. 5.7 pm).[17] Nozzle-to-plate distances were *ca*. 128 and 286 mm, yielding data in the s range 20−344 nm^{-1}; three usable plates were obtained at each distance. The sample and nozzle were held at *ca*. 296 K during the exposure periods.

The scattering patterns of benzene were also recorded for the purpose of calibration; these were analyzed in exactly the same way as those of the tetraborane(8) derivative so as to minimize systematic errors in the wavelengths and camera distances. Nozzle-to-plate distances, weighting functions used to set up the off-diagonal weight matrix, correlation parameters, final scale factors, and electron wavelengths for the measurements are collected in Table 1.

The electron-scattering patterns were converted into digital form using a computer-controlled Joyce-Loebl MDM6 microdensitometer with a scanning program described previously.[18] The programs used for data reduction[18] and least-squares refinement[19] have been described elsewhere; the complex scattering factors employed were those listed by Ross *et al*.[20]

Theoretical Calculations. Using the Gaussian series of programs,[21a,b] the two conformers of the *endo* and *exo* isomers of $B_4H_8PF_3$ with C_s symmetry were fully optimized at the HF/6-31G* level.[22] Analytical frequencies and zero-point energies (ZPE, scaled by 0.89)[22] for the stationary points on the potential-energy surface computed at the same level, followed by reoptimization of the geometries at the MP2/6-31G* level (*i.e*., with inclusion of electron correlation according to second-order Møller−Plesset perturbation theory and employing polarization functions on all atoms except hydrogen). The geometies of the lowest-energy conformers of $B_4H_8PF_3$, as well as those of the related species B_4H_{10} and 2,4-$(CH_2)_2B_4H_8$, were optmized at the MP2/TZP level, *i.e*. employing the following polarized triple-ζ basis set: B,F—Dunning's [5s3p] basis;[23] H—Dunning's [3s] basis;[23] P—McLean and Chandler's [6s5p] basis[24] augmented with one set of d-polarization functions on B, F, and P (exponents 0.386, 1.0, and 0.465, respectively) and with one set of p-polarization functions on hydrogen (exponent 0.75).

Higher-level optimizations were performed for PF_3 (MP2/TZ2Pf, *i.e*. with the same triple-ζ basis set described above, augmented with two sets of d- and one set of f-polarization functions on each atom: d-exponents of 0.652 and 0.216 on P and 3.107 and 0.855 on F; f-exponents of 0.452 and 1.917 for P and F, respectively), as well as for 2,4-$(CH_2)_2B_4H_8$ and B_4H_{10} (MP3/TZP, *i.e*. including electron correlation up to third-order Møller−Plesset perturbation theory). In addition, B_4H_{10} was optimized at the CCSD(T)/TZP level (*i.e*., including electron correlation to the coupled-cluster level[21c] with single, double, and perturbatively-included connected triple excitations.[25] Energies are denoted "level of calculation//level of geometry optimization".

NMR chemical shifts were computed using the the IGLO (individual gauge for localized orbitals) method[9] in its so-called "direct" implementation,[10] employing basis II, *i.e*. the following contracted Huzinaga[26] basis set: B,F [5s4p] augmented with one set of d-polarization functions (exponents 0.7 and 1.0 for B and F, respectively); P [7s6p] augmented with two sets of d-polarization functions (exponents 0.35 and 1.40); H [3s] augmented with one set of p-polarization functions (exponent 0.65).[9c] Theoretical ^{11}B chemical shifts were referenced to B_2H_6 and converted to the standard $BF_3{\cdot}OEt_2$ scale as described elsewhere.[11] The MP2/6-31G* geometry and IGLO ^{11}B NMR shifts were reported previously for *endo*-$B_4H_8PF_3$.[8]

Model

On the basis of the NMR evidence,[4,16] the results of the *ab initio* computations (see below), and a series of test refinements, the molecular model used to generate the atomic coordinates for $B_4H_8PF_3$ assumed the presence of the *endo* conformer only in the vapor. The structure was based upon the B_4H_{10} "butterfly" motif (see Figure 1) with the PF_3 group replacing the $H(1)_{endo}$ atom at the hinge position and no bridging hydrogen atoms at B(1). Throughout the analysis, the structure was

(13) For example, see: (a) Brain, P. T.; Hnyk, D.; Rankin, D. W. H.; Bühl, M.; Schleyer, P. v. R. *Polyhedron* **1994**, *13*, 1453. (b) Brain, P. T.; Rankin, D. W. H.; Robertson, H. E.; Alberts, I. L.; Schleyer, P. v. R.; Hofmann, M. *Inorg. Chem*. **1994**, *33*, 2565. (c) Hnyk, D.; Brain, P. T.; Rankin, D. W. H.; Robertson, H. E.; Greatrex, R.; Greenwood, N. N.; Kirk, M.; Bühl, M.; Schleyer, P. v. R. *Inorg. Chem*. **1994**, *33*, 2572. (d) Brain, P. T.; Bühl, M.; Fox, M. A.; Greatrex, R.; Leuschner, E.; Picton, M. J.; Rankin, D. W. H.; Robertson, H. E. *Inorg. Chem*. **1995**, *34*, 2841.

(14) Spielman, J. R.; Burg, A. B. *Inorg. Chem*. **1963**, *2*, 1139.

(15) Norman, A. D.; Schaeffer, R. *J. Am. Chem. Soc*. **1966**, *88*, 1143.

(16) Greatrex, R.; Fox, M. A. Unpublished results of a low-temperature ^{1}H and ^{11}B NMR study.

(17) Huntley, C. M.; Laurenson, G. S.; Rankin, D. W. H. *J. Chem. Soc., Dalton Trans*. **1980**, 954.

(18) Cradock, S.; Koprowski, J.; Rankin, D. W. H. *J. Mol. Struct*. **1981**, *77*, 113.

(19) Boyd, A. S. F.; Laurenson, G. S.; Rankin, D. W. H. *J. Mol. Struct*. **1981**, *71*, 217.

(20) Ross, A. W.; Fink, M.; Hilderbrandt, R. In *International Tables for Crystallography*; Wilson, A. J. C., Ed.; Kluwer Academic Publishers: Dordrecht, The Netherlands, Boston, MA, and London, 1992; Vol. C, p 245.

(21) (a) Frisch, M. J.; Trucks, G. W.; Schlegel, H. B.; Gill, P. M. W.; Johnson, B. G.; Wong, M. W.; Foresman, J. B.; Robb, M. A.; Head-Gordon, M.; Replogle, E. S.; Gomperts, R.; Andres, J. L.; Raghavachari, K.; Binkley, J. S.; Gonzalez, C.; Martin, R. L.; Fox, D. J.; Defrees, D. J.; Baker, J.; Stewart, J. J. P.; Pople, J. A. *Gaussian 92/DFT*, Revision F.4; Gaussian, Inc.: Pittsburgh, PA, 1993. (b) Frisch, M. J.; Trucks, G. W.; Schlegel, H. B.; Gill, P. M. W.; Johnson, B. G.; Robb, M. A.; Cheeseman, J. R.; Keith, T.; Petersson, G. A.; Montgomery, J. A.; Raghavachari, K.; Al-Laham, M. A.; Zakrzewski, V. G.; Ortiz, J. V.; Foresman, J. B.; Peng, C. Y.; Ayala, P. Y.; Chen, W.; Wong, M. W.; Andres, J. L.; Replogle, E. S.; Gomperts, R.; Martin, R. L.; Fox, D. J.; Binkley, J. S.; Defrees, D. J.; Baker, J.; Stewart, J. P.; Head-Gordon, M.; Gonzalez, C.; Pople, J. A. *Gaussian 94*, Revision B.3; Gaussian, Inc.: Pittsburgh, PA, 1995. (c) The coupled-cluster optimization was performed employing the program ACES II: Stanton, J. F.; Gauss, J.; Watts, J. D.; Lauderdale, W. J.; Bartlett, R. J. *Int. J. Quantum Chem. Symp*. **1992**, *26*, 879.

(22) Hehre, W.; Radom, L.; Schleyer, P. v. R.; Pople, J. A. *Ab initio Molecular Orbital Theory*; Wiley: New York, 1986.

(23) Dunning, T. H. *J. Chem. Phys*. **1970**, *53*, 2823.

(24) MacLean, A. D.; Chandler, G. S. *J. Chem. Phys*. **1980**, *76*, 163.

(25) (a) Purvis, G. D.; Bartlett, R. J. *J. Chem. Phys*. **1982**, *76*, 1910. (b) Scuseria, G. E.; Janssen, C. L.; Schaefer, H. F., III. *J. Chem. Phys*. **1988**, *89*, 7382. (c) Scuseria, G. E.; Schaefer, H. F., III. *J. Chem. Phys*. **1989**, *90*, 3700.

(26) Huzinaga, S. *Approximate Atomic Wave Functions*; University of Alberta: Edmonton, Canada, 1971.

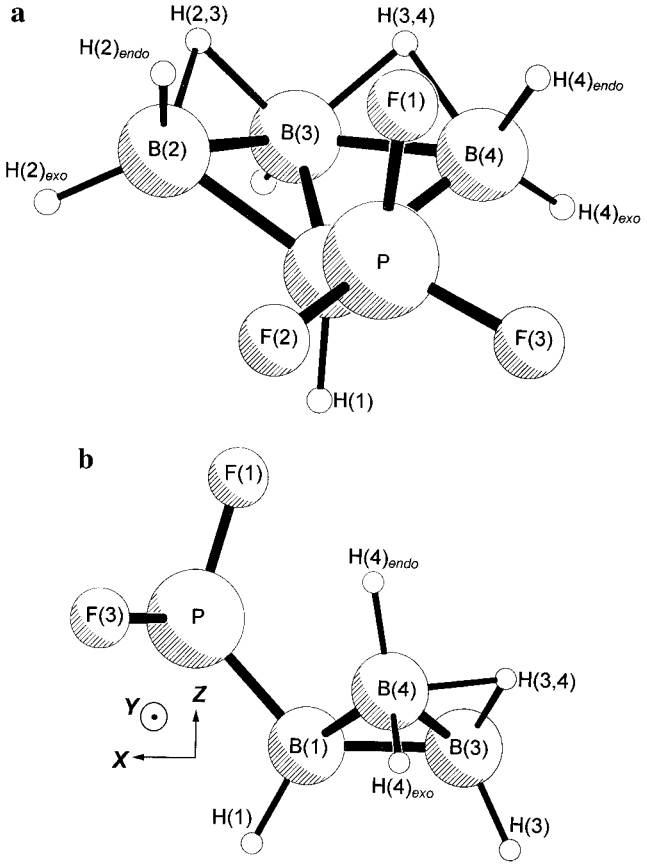

Figure 1. Views of *endo*-$B_4H_8PF_3$ in the optimum refinement of the electron-diffraction data: (a) perspective view; (b) view perpendicular to the molecular C_s plane.

Table 2. Structural Parameters (r_α°) for *endo*-$B_4H_8PF_3$ (Distances/pm; Angles/deg)[a,b]

param		
p_1	$^1/_5\{r$[B(1)−B(3)] + 2r[B(2)−B(3)] + 2r[B(1)−B(2)]}	180.3(8)
p_2	$^1/_2\{r$[B(1)−B(2)] + r[B(2)−B(3)]} − r[B(1)−B(3)]	10.1(8)
p_3	r[B(1)−B(2)] − r[B(2)−B(3)]	4.8(9)
p_4	r[B(1)−P]	179.8(9)
p_5	$^1/_3\{r$[P−F(1)] + 2r[P−F(2)]}	152.8(1)
p_6	r[P−F(2)] − r[P−F(1)]	0.8(f)
p_7	r[B−H](mean)	125.5(9)
p_8	r[B−H_t](mean) − r[B−H_b](mean)	−13.6(9)
p_9	r[B(3)−H(2,3)] − r[B(2)−H(2,3)]	5.8(25)
p_{10}	"butterfly angle" B(1)B(2)B(3)/B(1)B(4)B(3)	133.9(23)
p_{11}	B(3)B(1)P	131.6(11)
p_{12}	"C_3 axis"−P−F	117.6(1)
p_{13}	PF_3 tilt	−3.5(11)
p_{14}	PB(1)H(1)	108.5(18)
p_{15}	B(1)B(3)H(3)	115.0(f)
p_{16}	origin−B(2)−H(2)$_{endo/exo}$/yz	121.3(f)
p_{17}	B(1)B(2)B(3)/B(2)H(2,3)B(3)	19.7(f)
p_{18}	PF_3 twist	0.0(f)
p_{19}	% B_4H_8CO	3.5(f)

[a] For definitions of parameters, see the text. [b] Figures in parentheses are the estimated standard deviations. f = fixed.

assumed to have C_s symmetry, although this assumption was tested in the final refinements. With the origin of the coordinate system chosen to lie on B(1)−B(3) such that the y axis passed through B(2)···B(4), the model for $B_4H_8PF_3$ was described by the parameters listed in Table 2, with the atom-numbering scheme as shown in Figure 1.

The B_4 cage was defined by four geometrical parameters: a weighted mean of all bonded B−B distances (p_1), the difference between the average hinge−wing and the hinge−hinge B−B distances (p_2), the difference between the two hinge−wing B−B distances (p_3), and the "butterfly" angle (p_{10}) defining the angle between the planes B(1)B(2)B(3) and B(1)B(4)B(3).

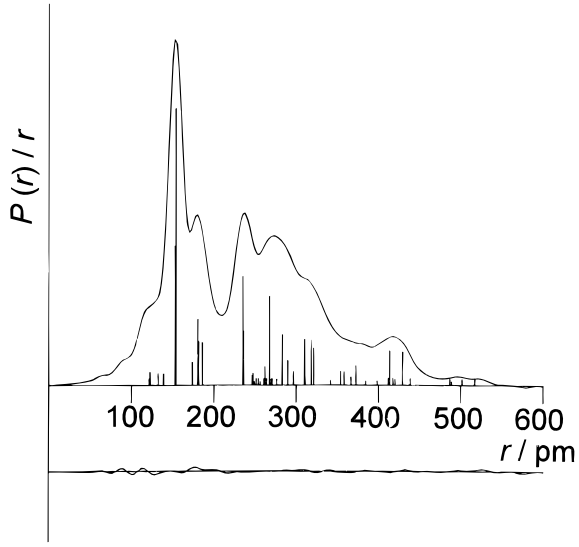

Figure 2. Observed and final weighted difference radial-distribution curves for *endo*-$B_4H_8PF_3$. Before Fourier inversion the data were multiplied by $s\cdot\exp[(-0.00002s^2)/(Z_F - f_F)(Z_B - f_B)]$.

For the PF_3 group, the two very similar P−F distances were defined by a weighted mean (p_5) and a difference (p_6). The F atoms were located assuming all FPF angles to be equal. Thus, a pseudo-C_3 axis, P−O, was defined for the PF_3 group such that P−O lay in the B(3)B(1)P plane, yielding all B(1)PF angles identical when P−O was coaxial with P−B(1). The PF_3 tilt (p_{13}) described the angle B(1)PO, *i.e.* the angle between B(1)−P and the pseudo-C_3 axis, such that an increasing tilt resulted in a decreasing B(1)PF(1) angle. Rotation of the PF_3 group about P−O from a starting position (0°) with F(1)PB(1)H(1) = 180° was allowed by p_{18}.

The positions of the hydrogen atoms were defined by seven refinable parameters. The B−H distance parameters consisted of the mean of the terminal (H_t) and bridging (H_b) distances (p_7), a difference between the average terminal and the average bridging distances (p_8), and the difference between the two different B−H_b distances (p_9). For the four slightly different B−H_t distances, the differences from the weighted mean value were fixed at the theoretical (MP2/6-31G* level) values. H(1) and H(3) were located in the B(3)B(1)P plane *via* the angles PB(1)H(1) (p_{14}) and B(1)B(3)H(3) (p_{15}), respectively. The H(2)$_{exo}$ and H(2)$_{endo}$ atoms were located initially in the yz plane [containing B(2) and B(4); see Figure 1] by the angle H(2)−B(2)−origin (p_{16}), and the BH_2 unit was positioned by three nonrefinable parameters: in the plane by a small wag angle and out of the plane by small rock and twist angles. These angles were fixed at the theoretical values. Finally, the bridging atoms H(2,3) and H(3,4) were allowed to move out of the B(1)B(3)B(2) and B(1)B(3)B(4) planes, respectively, becoming more *endo* with increasing p_{17}.

Refinement

The radial-distribution curve for $B_4H_8PF_3$ (Figure 2) shows three features in the bonding region, two peaks at *ca*. 153 and 177 pm and a shoulder at *ca*. 120 pm. These are assigned to the P−F distances, the B−P and B−B distances, and the B−H (H_t and H_b) distances, respectively. Above 200 pm, the most intense peak lies at *ca*. 235 pm and is associated with the F···F nonbonded pairs. The peak at *ca*. 270 pm arises from scattering from the B(2)···P, B(1)···F, and B(2)···B(4) nonbonded pairs

while the broad shoulder centered at *ca*. 312 pm corresponds to the B(2)···F and B(3)···P nonbonded pairs. The peak at *ca*. 415 pm originates mainly from scattering by the B(2)···F(3) and B(2)···F(2) nonbonded pairs, and the weak broad feature at *ca*. 500 pm consists principally of four-bond F···H contributions.

The $r_\alpha°$ structure of $B_4H_8{\cdot}PF_3$ was refined. A harmonic vibrational force field was computed at the HF/6-31G* level, and the Cartesian force constants were transformed into those described by a set of symmetry coordinates using the program ASYM40.[27] Because a full analysis of experimental vibrational frequencies is not available for the compound, it was not possible to scale the theoretical force constants on this basis. Instead, as the best alternative, empirical scale factors of 0.9 for bond stretches, 0.85 for bends, and 0.8 for torsions were employed.[28] Values for the root-mean-square amplitudes of vibration (u) and perpendicular amplitude corrections (K) were then derived from the scaled force constants using ASYM40.[27]

Using starting values taken from the structure optimized *ab initio* at the MP2/6-31G* level, it was possible to refine six of the parameters defining the heavy atom and also the average B−H_t distance. Introducing parameters defining differences between bond lengths, *e.g.* p_2, p_3, p_8, and p_9, either caused the refinement to become unstable (large oscillations in the R_G factor between cycles) or led such parameters to adopt unrealistic values. Attempts were made subsequently to refine these parameters using flexible restraints.[29,30]

Flexible restraints may allow the refinement of parameters that would otherwise have to be fixed. Estimates of the values of these restrained quantities and their uncertainties are used as additional observations in a combined analysis similar to those routinely carried out for electron-diffraction data combined with rotation constants and/or dipolar coupling constants.[31] The values and uncertainties for the extra observations are derived from another method such as X-ray diffraction or theoretical computation. *All* geometrical parameters are then included in the refinements. In cases where a restraint corresponds exactly to a refined parameter, if the intensity pattern contains useful information concerning the parameter, it will refine with an esd less than the uncertainty in the corresponding additional observation. However, if there is essentially no relevant information, the parameter will refine with an esd equal to the uncertainty of the extra observation and its refined value will equal that of the restraint. In this case, the parameter can simply be fixed, in the knowledge that doing this does not influence either the magnitudes or the esd's of other parameters. In some cases, because increasing the number of refining parameters allows all effects of correlation to be considered, some esd's may increase. Overall, this approach utilizes all available data as fully as possible and returns more realistic esd's for refining parameters; the unknown effects of correlation with otherwise fixed parameters are revealed and included.

Using flexible restraints, it was possible to refine the four bond-distance differences listed above. These were restrained directly with the values $p_2 = 11.3 \pm 1.0$ pm, $p_3 = 5.1 \pm 1.0$ pm, $p_8 = -13.1 \pm 1$ pm, and $p_9 = 5.8 \pm 2.5$ pm. The angle PB(1)H(1) (p_{14}) was also refined subject to a flexible restraint of $109 \pm 2°$.

In addition, nine amplitudes of vibration were included in the final refinements, with just one restraint of u_7(B−H_t) to 8.5 ± 1.0 pm.

Lowering the molecular symmetry to C_1 by refinement of p_{21}, with the B_4H_6P skeleton being assumed to retain C_s symmetry, led to a slight reduction in R_G (0.003) and a refined PF_3 twist angle of 2.0(20)°. Changes in other refining parameters were all within 1 esd of their values for $p_{21} = 0°$. Since the refined value is not significantly different from 0°, it was subsequently fixed at 0° in the final refinements.

The ^{11}B NMR spectrum of the sample of $B_4H_8PF_3$ showed the presence of a small amount of B_4H_8CO, estimated at <5%. Therefore, further refinements were undertaken allowing for the presence of this impurity in the diffracted vapor. The structure for B_4H_8CO was taken from the GED analysis,[6] which assumed two conformers, *viz*. 62% *endo* and 38% *exo*. A plot of the variation of R_G with p_{19}, the fraction of B_4H_8CO present, showed a minimum at *ca*. 3.5% (curve-fitted using a fourth-order polynomial); at the 95% confidence level,[32] the error was 1.5%, indicating an esd of *ca*. 0.8%. Thus, in the final refinements, p_{19} was fixed at 0.035. However, even with $p_{19} = 0.1$, there were no significant changes in the refining geometrical parameters compared to those obtained with $p_{19} = 0.0$, the change in R_G being associated with small changes in some of the refining amplitudes of vibration. This further vindicates our use of a model defining only one conformer for $B_4H_8PF_3$; the inclusion of small amounts of "impurities" such as B_4H_8CO has no significant effect on the values of the final refined geometrical parameters in the GED analysis.

Values of the principal interatomic distances for the final refinement ($R_G = 0.065$, $R_D = 0.043$) are listed in Table 3, and the most significant values of the least-squares correlation matrix are given in Table 4. The experimental and difference radial-distribution curves are shown in Figure 2, and the molecular-scattering intensities, in Figure 3. Cartesian coordinates are included as part of the Supporting Information.

Results and Discussion

As assessed by ^{19}F and ^{11}B NMR spectroscopy,[4,16] $B_4H_8PF_3$ exists as a mixture of two isomers, *endo* and *exo*. The *endo* form is predominant in solution, and only small amounts of the *exo* isomer are present. In order to see if a significant proportion of the *exo* form might be expected in the gas phase, we performed *ab initio* computations for the geometries and energies of both isomers. At the MP2/TZP//MP2/TZP + ZPE-(HF/6-31G*) level, the *exo* form is computed to lie 9.3 kJ mol^{-1} higher in energy than the *endo* isomer, corresponding to an *endo*:*exo* ratio of *ca*. 98:2 at room temperature.

Ab initio (r_e) and experimental ($r_\alpha°$) geometrical parameters for $B_4H_8PF_3$ are compared in Table 5. The MP2/6-31G* level and GED data for the *endo* conformer are in only moderately good agreement. In particular, the computed average P−F distances are significantly overestimated [MP2/6-31G*, 156.9 *vs* GED, 152.8(1) pm], and the B−B distances of the borane framework are somewhat underestimated [B−B(mean): MP2/6-31G*, 178.5 *vs* GED, 180.3(8) pm]. A similar disparity for certain B−B separations has been noted for other tetraborane-

(27) ASYM40 is an updated version of ASYM20: Hedberg, L.; Mills, I. M. *J. Mol. Spectrosc*. **1993**, *160*, 117.
(28) For example, see: (a) Pulay, P.; Fogarasi, G.; Pongor, G.; Boggs, J. E.; Vargha, A. *J. Am. Chem. Soc*. **1983**, *105*, 7037. (b) Rauhut, G.; Pulay, P. *J. Phys. Chem*. **1995**, *99*, 3093 and references therein.
(29) Blake, A. J.; Brain, P. T.; McNab, H.; Miller, J.; Morrison, C. A.; Parsons, S.; Rankin, D. W. H.; Robertson, H. E.; Smart, B. A. *J. Phys. Chem*. **1996**, *100*, 12280.
(30) (a) Mitzel, N. W.; Smart, B. A.; Parsons, S.; Robertson, H. E.; Rankin, D. W. H. *J. Chem. Soc., Perkin Trans. 2* **1996**, 2727. (b) Brain, P. T.; Morrison, C. A.; Parsons, S.; Rankin, D. W. H. *J. Chem. Soc., Dalton Trans*. **1996**, 4589.
(31) For example, see: Abdo, B. T.; Alberts, I. L.; Attfield, C. J.; Banks, R. E.; Blake, A. J.; Brain, P. T.; Cox, A. P.; Pulham, C. R.; Rankin, D. W. H.; Robertson, R. E.; Murtagh, V.; Heppeler, A.; Morrison, C. *J. Am. Chem. Soc.* **1996**, *118*, 209.
(32) Hamilton, W. C. *Acta Crystallogr*. **1965**, *18*, 502.

Table 3. GED Interatomic Distances (r_a/pm) and Amplitudes of Vibration (u/pm) for *endo*-$B_4H_8PF_3$[a,b]

		dist	amplitude
r_1	B(1)−B(3)	173.4(12)	6.2
r_2	B(1)−B(2)	185.8(9)	7.5
r_3	B(2)−B(3)	181.2(10)	6.8 } f
r_4	B(1)−P	180.1(9)	5.5
r_5	P−F(1)	152.7(1)	4.3 (tied to u_6)
r_6	P−F(2)	153.8(1)	4.3(2)
r_7	B(2)−H(2)$_{exo}$	122.2(9)	8.7(9)
r_8	B(2)−H(2)$_{endo}$	122.7(9)	8.8
r_9	B(3)−H(3)	121.3(9)	8.7 } (tied to u_7)
r_{10}	B(1)−H(1)	121.6(9)	8.8
r_{11}	B(3)−H(3,4)	132.4(16)	9.7 } f
r_{12}	B(4)−H(3,4)	138.9(18)	11.0
r_{13}	F(1)···F(2)	235.1(2)	7.1(2)
r_{14}	F(2)···F(3)	235.8(2)	6.9 (tied to u_{13})
r_{15}	B,P···H (two bond)	246.5−276.2	10.8−13.3
r_{16}	B(2)···P	267.3(6)	8.7(8)
r_{17}	B(1)···F(2)	282.9(8)	8.4(11)
r_{18}	B(1)···F(1)	289.6(21)	7.9 (tied to u_{17})
r_{19}	B(2)···B(4)	296.8(22)	9.1 (f)
r_{20}	B(3)···P	321.2(10)	8.2(5)
r_{21}	B,P···H (three bond)	261.9−420.0	12.0−22.8
r_{22}	B(2)···F(1)	310.2(32)	15.3
r_{23}	B(2)···F(2)	318.3(9)	19.8 } tied to u_{20}
r_{24}	B(3)···F(1)	372.7(19)	14.9(26)
r_{25}	B(2)···F(3)	413.5(5)	11.1(9)
r_{26}	B(3)···F(2)	429.2(12)	12.0 (tied to u_{25})

[a] For atom-numbering scheme, see Figure 1. Figures in parentheses are the estimated standard deviations; f = fixed. [b] F···H and H···H nonbonded distances were also included in the refinements but are not listed here.

Table 4. Least-Squares Correlation Matrix (×100) for the GED Refinement

p_4	p_{10}	p_{11}	p_{12}	p_{13}	u_{16}	u_{17}	u_{20}	u_{25}	k_1	k_2	
-79									55		p_1
		53									p_2
	58	-52			-61	-61					p_4
			54								p_5
									-64		p_7
		-78		-57		-67	63	57			p_{10}
				68		68	-55	-51			p_{11}
						64	-68				p_{13}
										89	u_6
										52	u_{13}
					69					51	u_{17}

[a] Only elements with absolute values >50 are shown. k_1 and k_2 are scale factors.

(8) derivatives and has been ascribed tentatively to a slight shortfall in the particular levels employed in the *ab initio* computations.[13d]

In order to identify possible shortcomings of the MP2/6-31G* geometries, we performed higher-level geometry optimizations for the title compound, as well as for tetraborane(10), B_4H_{10},[30,33] and 2,4-dimethylenetetraborane(8), 2,4-$(CH_2)_2B_4H_8$.[13c] The cage B−B-bonded distances are summarized in Table 6. On going from MP2/6-31G* to MP2/TZP, all B−B distances increase by *ca.* 1−3 pm, resulting in improved agreement with the GED values. Levels of electron correlation higher than MP2 affect the B−B distances less, up to *ca.* 1.6 pm (compare MP2/TZP and MP3/TZP or CCSD(T)/TZP entries in Table 6). Remaining deficiencies in the theoretical geometries are probably due to basis set effects and should be small. Note that experimental distances are for a vibrationally-averaged rather than a theoretical equilibrium structure and that some experimental values are associated with large uncertainties, particularly B(1)−B(3) distances.

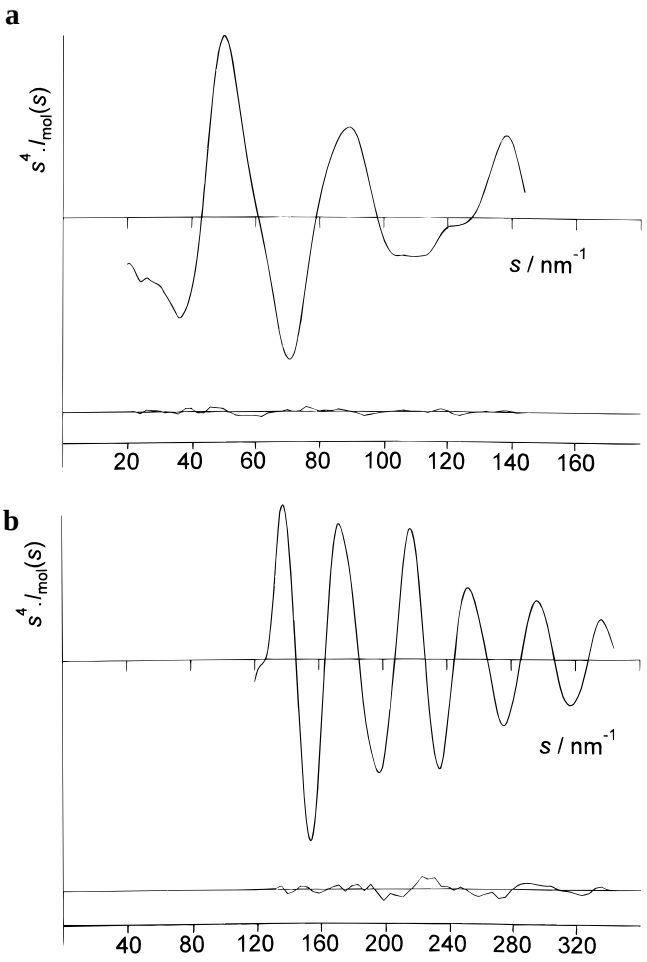

Figure 3. Observed and final weighted difference molecular-scattering intensity curves for *endo*-$B_4H_8PF_3$. Nozzle-to-plate distances: (a) 286 mm; (b) 128 mm.

Table 5. Comparison of Theoretical (r_e) and Experimental ($r_\alpha°$) Geometrical Parameters for $B_4H_8PF_3$[a]

	MP2/6-31G* [b]		MP2/TZP		GED[c]
distance/angle	*endo*	*exo*	*endo*	*exo*	*endo*
B(1)−B(3)	169.5	170.6	170.4	171.5	172.2(12)
B(1)−B(2)	183.3	181.1	184.8	182.2	184.7(9)
B(2)−B(3)	178.2	178.2	179.7	179.7	179.9(10)
B(1)−P	180.2	183.2	181.0	183.7	179.8(9)
P−F(1)	156.4	156.5	156.1	156.3	152.2(1)[e]
P−F(2)	157.2	156.9	157.1	156.8	153.0(1)[e]
B(3)−H(3,4)	129.6	129.1	130.0	129.6	130.7(16)
B(4)−H(3,4)	135.4	136.5	136.0	137.0	136.5(18)
B−H_t (mean)	119.4	119.3	119.2	119.2	120.0(9)
"butterfly" angle[d]	136.6	143.4	136.1	142.8	133.9(23)
B(3)B(1)P	131.6	249.9	131.3	249.7	131.6(11)

[a] For atom-numbering scheme, see Figure 1. Distances are given in picometers and angles in degrees. Figures in parentheses are the estimated standard deviations of the last digits. [b] Identical within 0.1 pm to the data reported in ref 8. [c] For r_a distances, see Table 3. [d] Angle between planes B(1)B(2)B(3) and B(1)B(2)B(4). [e] The difference between P−F distances was fixed.

(33) Dain, C. J.; Downs, A. J.; Laurenson, G. S.; Rankin, D. W. H. *J. Chem. Soc., Dalton Trans.* **1981**, 472.

Table 6. Cage B−B Distances (pm) for Tetraborane(10) Derivatives[a,b]

	B_4H_{10}		2,4-$(CH_2CH_2)B_4H_8$		*endo*-$B_4H_8PF_3$			*endo*-B_4H_8CO		
method[c]	B(1)−B(2)	B(1)−B(3)	B(1)−B(2)	B(1)−B(3)	B(1)−B(2)	B(2)−B(3)	B(1)−B(3)	B(1)−B(2)	B(2)−B(3)	B(1)−B(3)
MP2/6-31G*	183.5	171.4	185.9	171.3	183.3	178.2	169.5	185.1	178.0	169.9
MP2/TZP	185.6	173.1	188.2	173.3	184.8	179.7	170.4	187.0	179.7	171.4
MP3/TZP	186.9	173.8	189.8	173.6						
CCSD(T)/TZP	186.5	173.4								
GED	186.5(2)	173.6(5)	189.5(3)	172.9(17)	185.8(9)	181.2(10)	173.4(12)	184.9(4)	178.0(6)	172.7(10)

[a] Values in parentheses are the estimated standard deviations. [b] For references, see the text. [c] Theoretical distances are r_e; GED parameters are r_a.

Table 7. Computed Chemical Shifts (IGLO, Basis II) and Relative Energies of Theoretical and Experimental Structures for *endo*-$B_4H_8PF_3$[a]

	$\delta(^{11}B)$[b]			rel energy[c]/ kJ mol^{-1}
geometry	B(1)	B(2,4)	B(3)	MP2/TZP
MP2/6-31G*[d]	−58.9(−55.0)	−3.7(−3.5)	2.1(1.1)	0.8(12.5)
MP2/TZP	−58.2(−54.5)	−3.3(−3.1)	2.5(1.6)	0.0(11.8)[f]
GED (r_a)	−58.8	−1.6	3.5	12.9
GED ($r_\alpha°$)	−59.4	−2.3	3.0	12.6
experimental[e]	−58.6(−55.5)	−4.1(n.o.)	1.5(−1.5)	

[a] Values in parentheses are for the *exo* conformer. [b] Relative to $BF_3{\cdot}OEt_2$. [c] Energy of the structure relative to the MP2/TZP fully optimized geometry. [d] The IGLO values for the *endo* conformer differ slightly (up to *ca*. 1 ppm) from those reported in ref 8, since we employed a slightly larger basis set (polarized triple-ζ quality for the hydrogen atoms). [e] In $CDCl_3$. This work; n.o. = not observed due to overlapping peaks. [f] The energy difference (*endo*−*exo*), corrected for zero-point energy (HF/6-31G* scaled by 0.9) = 9.3 kJ mol^{-1}, equivalent to a ratio of conformers of 98:2, *endo*:*exo*, at 296 K.

Unlike the B−B separations, the P−F distances (Table 5) change very little on going from the MP2/6-31G* to the MP2/TZP optimized theoretical geometry. Surprisingly for such a small molecule, the P−F bond length in free PF_3 is also considerably overestimated at these levels; *cf*. 159.5 (MP2/6-31G*) and 160.0 (MP2/TZP) *vs* 156.3(1) pm (MW, r_e).[34,35] The error in the *ab initio* bond length is somewhat reduced when a larger basis set is employed; *cf*. the MP2/TZ2P(f) value of 157.9 pm. While higher levels of electron correlation such as CCSD(T) have only negligible effects on the PF_3 geometry,[36] even larger basis sets are probably required for a quantitative description. It is not clear why the P−F bond length in PF_3 appears to be so demanding with respect to the theoretical level employed. Nevertheless, all theoretical methods and the experimental results agree that the P−F bond length in PF_3 decreases by *ca*. 3 pm upon formation of the B_4H_8 adduct.

In other joint experimental and *ab initio* studies of borane and heteroborane derivatives,[13] we have assessed the accuracy of the experimental geometries by means of *ab initio* computations of their ^{11}B chemical shifts and of their relative (or "excess") energies with respect to the optimized structures.[11] The corresponding results for $B_4H_8PF_3$ are shown in Table 7. Despite the geometrical variations discussed above, all theoretical and experimental geometries of $B_4H_8PF_3$ perform about equally well in the chemical-shift computations; the $\delta(^{11}B)$ values computed for the various structures agree very well with the experimental data, within *ca*. 2 ppm.[37]

The relative energy of an experimental geometry is always greater than that of its structure optimized *ab initio*.[11,22] However, large "excess" energies (50 kJ mol^{-1} or more, depending on the size of the system) can help to identify experimental "problem cases".[11,13a] The "excess" energies of the experimental structures of $B_4H_8PF_3$ are relatively small, *ca*. 13 kJ mol^{-1} (Table 7). In each case studied so far,[13] the largest part of such "excess" energy has been attributed to the different positions of the hydrogen atoms in the theoretical (r_e) and experimental (r_a, *etc*.) structures. This can be assessed by calculating relative energies of so-called "H-relaxed" GED geometries, where the heavy-atom skeleton is fixed at the experimental geometry and the positions of the hydrogens are optimized. During such an MP2/6-31G* level optimization for the $r_\alpha°$ structure of $B_4H_8{\cdot}PF_3$, the energy dropped by *ca*. 1 kJ mol^{-1}. The major part of the "excess" energy of this molecule, however, is due to the overestimation of the P−F bond lengths in the *ab initio* structure; an "H,F-relaxed" $r_\alpha°$ GED structure, *i.e*. with both H and F positions optimized at the MP2/6-31G* level, lies only 1.3 kJ mol^{-1} above the fully optimized minimum. Thus, judging from the experimental and theoretical criteria (*R* values, computed chemical shifts, and relative energies), the joint *ab initio*/GED geometry offers an accurate and reliable description of the molecular structure of *endo*-$B_4H_8PF_3$.

The computed association energy of B_4H_8 with PF_3 to form *endo*-$B_4H_8PF_3$ is −97.1 kJ mol^{-1} at the MP2/6-31G*//MP2/6-31G* + ZPE(HF/6-31G*) level, *i.e*. somewhat larger than that of the $BH_3 + PF_3 \rightarrow BH_3{\cdot}PF_3$ reaction, −92.0 kJ mol^{-1} (the experimental $\Delta H°$ is −96 kJ mol^{-1}).[38] Comparable Lewis acid behaviors of B_4H_8 and BH_3 toward CO have been noted.[7] However, there is experimental evidence from competition experiments that the B_4H_8 group behaves as a stronger Lewis acid toward halodifluorophosphines, including PF_3.[1]

In addition to geometrical isomers (*endo* and *exo*), rotational isomers about the B−P bond have been detected in the low-temperature NMR spectra of some B_4H_8 adducts with halodifluorophosphines; rotamers are found for *endo*, but not for *exo*, isomers.[4] To estimate the corresponding potential-energy barriers, we located the transition-state structures (MP2/6-31G* level) for rotation of the PF_3 groups. For both *endo*- and *exo*-$B_4H_8PF_3$, the transition-state geometries possess C_s symmetry, with a H(1)B(1)PF(1) dihedral angle of 0°, *i.e*. with PF_3 in Figure 1 rotated by 60°. At the MP2/6-31G*//MP2/6-31G* + ZPE(HF/6-31G*) level, a barrier of 27.3 kJ mol^{-1} is computed for the *endo* conformer, but only 1.0 kJ mol^{-1} is computed for the *exo* conformer, consistent with the experimental observations.[4]

Of the tetraborane(8) derivatives carrying substituents at the hinge borons,[1−6,8] two others have been structurally characterized, *viz*. B_4H_8CO, in the gas phase by electron diffraction,[6] and $B_4H_8PF_2NMe_2$, by X-ray diffraction.[5] The carbonyl exists as a 62:38 *endo*:*exo* mixture in the gas phase, and the phosphine

(34) Kawashima Y.; Cox, A. P. *J. Mol. Spectrosc*. **1977**, *65*, 319.
(35) The SCF/6-31G* geometry is (apparently fortuitously) in good accord with experiment. For example, see: Breidung, J.; Thiel, W. *J. Phys. Chem*. **1988**, *92*, 5597.
(36) Breidung, J. Unpublished results.
(37) This agreement is excellent if it is borne in mind that theoretical values for rigid, isolated molecules are being compared with experimental data for vibrating species in solution.
(38) Fehlner, T. P. In *Boron Hydride Chemistry*; Muetterties, E. L., Ed.; Academic Press: New York, 1975; Chapter 4, p 175.

adopts the *endo* conformation in the solid phase. Including the structure of $B_4H_8PF_3$, it is found that (i) the B_4H_8 cages are distorted consistently to C_s, or near C_s, symmetry relative to B_4H_{10},[30,33] with *r*[B(1)−B(2)] longer than *r*[B(2)−B(3)], and (ii) for the *endo* conformer, the "butterfly" angle is close to 135°, as compared to the much narrower angle of *ca*. 117° in B_4H_{10}. For the gas-phase structures, when PF_3 is replaced by CO, the experimental (and theoretical) B_4 cage geometrical parameters for the *endo* conformers change very little (see Tables 3 and 6).

In the gas phase at room temperature, $B_4H_8PF_3$ consists almost entirely of the *endo* conformer (*ab initio*, *endo* mole fraction = 0.98), in contrast to B_4H_8CO with an *endo* mole fraction of 0.62.[6] For each compound, although the substituent lies "preferentially" in the *endo* position, the "butterfly" angle is narrower in the *endo* than in the *exo* conformer: B_4H_8CO, 135(4)° *vs* 144.0(23)°, and $B_4H_8PF_3$, 133.9(23)° *vs* 142.8° (MP2/TZP optimization). Both observations point to the dominance of electronic bonding factors over steric interactions in realizing the structures of these compounds.

Experimentally-determined structural parameters for other trifluorophosphine−borane adducts are compared to those for *endo*-$B_4H_8PF_3$ in Table 8.[39−41] The P−B bond length is consistent with those found for similar adducts and, at r_g = 180.3(9) pm, appears to be the shortest reported to date. The reduction in electron density at the phosphorus atom on complexation is accompanied by a shortening of the P−F bonds and a widening of the FPF angle relative to free PF_3, in accord with the predictions of VSEPR theory.[42]

Acknowledgment. We thank the EPSRC for (i) financial support of the Edinburgh Electron Diffraction Service (Grant GR/K44411), including research fellowships to P.T.B. and H.E.R., (ii) provision of the microdensitometer facilities at the Daresbury Laboratory, and (iii) the award of a postdoctoral fellowship to M.A.F. (Grant GR/H3667). A.N. was supported by a studentship from the Ministry of Culture and Higher Education of the Islamic Republic of Iran, and M.B. gratefully acknowledges generous support from W. Thiel and the Fonds der Chemischen Industrie. We thank Dr. B. A. Smart (University of Edinburgh) for assistance with the force-field analysis, Dr. L. Hedberg (Oregon State University) for a copy of the program ASYM40, and Dr. J. Breidung (Universität Zürich) for helpful discussions and for providing unpublished computational results for PF_3. Calculations were performed on IBM RS6000 workstations at the Competence Center for Computational Chemistry, ETH Zürich, and on an NEC SX3 supercomputer at the Centro Svizzero di Calcolo Scientifico at Manno, Switzerland.

Table 8. Structural Parameters (*r*/pm, ∠/deg) for Borane−PF_3 Adducts[a]

compd	method[b]	*r*(P−B)	*r*(P−F)	∠FPF
$F_3P{\cdot}BH_3$	MW[39]	183.6(12)	153.8(8)	99.8(10)
$F_2PH{\cdot}BH_3$	MW[40]	183.2(9)	155.2(6)	100.0(5)
$(F_3P)_2B_2H_4$	GED[41]	185.0(28)	154.0(3)	101(2)
$B_4H_8PF_3$	GED[c]	180.3(9)	152.8(1)	100.2(1)
			153.9(1)	
PF_3	MW[34]		156.3(1)	97.7(1)

[a] Values in parentheses are the estimated standard deviations. [b] MW = microwave spectroscopy (r_o or r_s), GED = gas-phase electron diffraction (r_g). [c] This work.

Supporting Information Available: Listings of (i) atomic coordinates for the GED geometries and (ii) absolute energies, zero-point energy corrections, and atomic coordinates for the theoretically optimized geometries (2 pages). Ordering information is given on any current masthead page.

IC961032J

(39) Kuczowski, R. L.; Lide, D. R., Jr. *J. Chem. Phys*. **1967**, *46*, 1.
(40) Pasinski, J. P.; Kuczowski, R. L. *J. Chem. Phys*. **1971**, *54*, 1903.
(41) Lory, E. R.; Porter, R. F.; Bauer, S. H. *Inorg. Chem*. **1971**, *10*, 1072.
(42) Gillespie, R. J. *J. Chem. Educ*. **1970**, *47*, 18.